Received: 9 August 2021 | Revised: 7 April 2022 | Accepted: 25 April 2022

DOI: 10.1002/cpe.7167

RESEARCH ARTICLE

WILEY

Detection and categorization of acute intracranial hemorrhage subtypes using a multilayer DenseNet-ResNet architecture with improved random forest classifier

Balraj M. Monica Jenefer[1] | K. Senathipathi[2] | Aarthi[3] | Annapandi[4]

[1]Department of Computer Science and Engineering, Meenakshi Sundararajan Engineering College, Chennai, Tamil Nadu, India

[2]Department of Computer Science and Engineering, Sri Krishna College of Engineering and Technology, Coimbatore, Tamil Nadu, India

[3]Department of Computer Science and Engineering, Meenakshi Sundararajan Engineering College, Chennai, Tamil Nadu, India

[4]Department of Electrical and Electronics Engineering, Francis Xavier Engineering College, Tirunelveli, Tamil Nadu, India

Correspondence
Balraj M. Monica Jenefer, Department of Computer Science and Engineering, Meenakshi Sundararajan Engineering College, Chennai, Tamil Nadu, India.
Email: bmonica20@gmail.com

Summary

In this article, the detection and categorization of acute intracranial hemorrhage (ICH) subtypes using a multilayer DenseNet-ResNet architecture with improved random forest classifier (IRF) is proposed to detect the subtypes of intracerebral hemorrhage with high accuracy and less computational time. Here, the brain CT images are taken from the physionet repository publicly dataset. Then the images are preprocessed to eliminate the unwanted noises. After that, the image features are extracted by using multilayer densely connected convolutional network (DenseNet) combined with residual network (ResNet) architecture with multiple convolutional layers. The subtypes are epidural hemorrhage (EDH), subarachnoid hemorrhage (SAH), intraparenchymal hemorrhage (IPH), subdural hemorrhage (SDH), intraventricular hemorrhage (IVH) are classified by using an IRF classifier with high accuracy. The simulation process is carried out in MATLAB site. The proposed multilayer-DenseNet-ResNet-IRF attains higher accuracy 23.44%, 31.93%, 42.83%, 41.9% is compared with the existing methods, such as deep learning algorithm for automatic detection and classification of acute intracranial hemorrhages in head CT scans (ICH-DC-2D-CNN), fusion-based deep learning along nature-inspired algorithm for the diagnosis of intracerebral hemorrhage (ICH-DC-FSVM), and detection of intracranial hemorrhage on CT scan images using convolutional neural network (ICH-DC-CNN) and double fully convolutional networks (FCNs), respectively.

KEYWORDS

brain CT images, DenseNet, improved random forest classifier, intracranial hemorrhage, ResNet

1 | INTRODUCTION

Brain hemorrhage is one of the categories of stroke that is caused by the high blood pressure; it leads to breakage of brain tissues and bleeding.[1,2] The strokes are mainly caused by venous infarction, vascular abnormalities, trauma effects, tumor, therapeutic anticoagulation, and cerebral aneurysm.[3,4] Intracranial hemorrhage (ICH) is a dangerous disease resulting high mortality rate within the age of 15 to 24.[5,6] An acute ICH leads to loss of speech, weakness, or paralysis of one side of the body.[7,8] ICH contains five types of brain strokes, they are (i) epidural hemorrhage, (ii) subarachnoid hemorrhage, (iii) Intraparanchymal hemorrage (iv) subdural hemorrhage, (v) intraventricular hemorrhage.[5] This disease may be cured by finding what type of disease is affected in the brain while taking brain CT images with high accuracy within less computational time.[9-13] EDH, SDH, IPH type hemorrhages are cured by finding the early diagnosis of the diseases in the brain tissues. IVH and ICH diseases are seriously affects the brain and causes death to the human beings.[14,15] Previously, several methods were used to detect the brain ICH hemorrhages, they are, segmentation and

classification active contour, region growing with fuzzy c-means, k-means algorithms.[16,17] For classification, Bayesian classification, fuzzy C-means (FCM), and expectation maximization (EM) are used by using CT images, but these methods does not provide sufficient accuracy for differentiating gray matter from the white matter.[18,19] Then the detection and classification process are used to find the ICH in brain, but these methods also consists of several problems, such as (1) the continuation of interference and to removing skull regions, brain ventricles, soft tissue edema under brain CT images, (2) uncertain location of hemorrhage under several kinds, (3) the comparison of shape and texture among few hemorrhage sorts that leads to extract the unneeded or ineffective features.[20-22] Moreover, the previous methods did not classify the accurate bleeding positions in the brain. That's why, this work motivates to detect and classify the subtypes of brain ICH. The computer aided diagnosis (CAD) tool is necessary for specialist, because physical examination by radiologists is difficult and time consuming. The automatic detection and classification of intracranial hemorrhage is paramount importance.

From other industries, the healthcare sector is quite dissimilar. It offers exciting solution through good accuracy in medical imaging as well as key technique for future applications in the health sector after deep learning success in another real-world application. With the help of magnetic resonance imaging (MRI), automated brain tumor identification is a hard task owing to its size, complexity, location, and variability. Several approaches were presented in the literature to detect the brain stroke lesions, but the presented methods did not present adequate accuracy and increased the error rate. But still, there is a scope to design an appropriate method for developing and implementing a more effective classifying system for brain tumor. These draw backs have motivated to do this research work.

The major objective of this work is to improve the classification accuracy by decreasing the computational time. The CT images of head are utilized in a great extent to diagnose many neurological diseases, like acute traumatic brain injury (TBI), acute stroke, and ICH. In this article, one of the most crucial neurological abnormalities namely acute Intracranial Hemorrhage is detected and classified into various subtypes for easy identification and early diagnosis. Here, early diagnosis is the only way to control the mortality rate in patients suffering from this deadly disease.

The novelty of this article is that the proposed acute intracranial hemorrhage (ICH) subtype detection and classification approach using a multilayer ResNet-DenseNet architecture in consort with the improved random forest classifier (IRF) classifier (ICH-ResNet-DenseNet-IRF) method classifies the acute intracranial hemorrhage disease into epidural hemorrhage, subarachnoid hemorrhage, intracerebral hemorrhage, subdural hemorrhage, intraventricular hemorrhage, normal are classified by using improved random forest with high classification accuracy.

In this article, detection and categorization of acute intracranial hemorrhage (ICH) subtypes using a multilayer DenseNet-ResNet architecture with IRF classifier is proposed to detect the subtypes of ICH with high accuracy and less computational time.

The main contributions of this article are:

- A detection and categorization of acute intracranial hemorrhage (ICH) subtypes using a multilayer DenseNet-ResNet architecture with IRF classifier is proposed to detect the subtypes of ICH with high accuracy with less computational time.
- At first, preprocessing is applied to remove the unwanted noises from the raw CT image. Then, a DenseNet combined with ResNet architecture with multiple convolutional layers is employed to extract the features needed to classify the subtypes of acute ICH.
- Finally, an IRF classifier[23] is used in the classification stage to achieve high performance with improved classification accuracy.
- For training and validation, a physionet repository publicly available ICH CT image dataset[24] is employed and classifier with its efficient features extracted by proposed ResNet-DenseNet model categorizes the ICH into its corresponding subtypes (IPH, IVH, SDH, EDH, or SAH).
- Finally, the efficiency of the proposed approach is compared with the existing approaches to reveal the effectiveness based on its diagnosis time in an actual emergency situation.

Remaining article is organized as: Section 2 depicts the recent studies. Section 3 illustrates about the proposed detecting and categorizing of acute ICH subtypes using a multilayer DenseNet-ResNet architecture with IRF classifier approach. Section 4 demonstrates the results and discussion. Finally, Section 5 concludes the article.

2 | LITERATURE SURVEY

Among various investigation works based on detection and classification of ICH, some of the most recent research works are reviewed as follows:

Faried et al.[25] have presented a correlation among skull base fracture and Intracranial Hemorrhage through traumatic brain injury. Where, brain CT image datasets were collected from the head injury with skull base fracture (SBF) among the clinical symptoms and loss of consciousness by taking Glasgow coma score (GCS) for examination. The main objective of the presented method was to identify the correlation among SBF and ICH. The experimental results were classified in three basis: head injury with absence of ICH, head injury with particular intracranial hemorrhage, head injury with numerous intracranial hemorrhages. The accuracy is calculated from SBF at anterior fossa reported 69.40% with mild head injury (64.70%). The limitation was lesser accuracy.

Ye et al.[26] have presented an exact diagnosis of intracranial hemorrhage and subtypes 3D joint convolution with recurrent neural network (CNN-RNN) for ICH including five subtypes (Intraventricular, cerebral parenchymal, epidural, subdural, subarachnoid). The experimental results show the accuracy was about greater than 98%, but the time was increased.

Prinz et al.[27] have presented a clinical organization and result of mature patients through extracorporeal life support device. It was associated with Intra cerebral hemorrhage with neurocritical perception and evaluation. The intra cerebral hemorrhage (ICH) disease was detected and treated extracorporeal membrane oxygenation (ECMO) in the cause of respiratory or cardiac problem. Several neurosurgical assessment and management of affected patient's studies were investigated to control the hemorrhage disease for controlling the mortality rate. The disadvantage of the presented method was increased the error rate.

Rava et al.[28] have presented an evaluation of artificial intelligence algorithm for intracranial hemorrhage detection. The objective of the presented method was to find the accurate ICH detection by using artificial intelligence. The experimental results shows accuracy was 95% with the training and testing of detecting hemorrhage slices. The presented method has lesser accuracy and consumed more time.

Kishan Das Menon and Janardhan[29] have presented a model that utilizes set of imaging data given with radiologic society of North under collaboration using American Society members for Neuroradiology. It helps the medical society to recognize the position, and sort of bleeding, so that affected patients got treated rapidly and efficiently. The presented algorithm was made up of the framework of neural network intended to notice ICH while addressing various challenges, like comparatively the size of small hemorrhage and large variation inside the brain. The presented method does not support large dataset and accuracy was decreased.

Thirunavukkarasu et al.[30] have presented an intracranial hemorrhage detection with deep convolutional neural network (DCNN). Where, the diseases were recognized with the help of DCNN method as computed tomography (CT) scans for automatic brain hemorrhage recognition. The presented method was used to classify the subtypes of intracranial hemorrhage recognition and quantification of intraperitonal, subdural/epidural, and subarachnoid hemorrhage. DICOM datasets consists of 180 GB images of 3D head CT studies. The experimental results show the accuracy was about 96.1%. The limitation was the computational time was increased and the speed was reduced.

Cho et al.[31] have presented an improvement of the sensitivity in the recognition and delimitation of the intracranial hemorrhage lesion with cascade deep learning models. A cascading deep learning approach built with two CNNs and double fully convolutional networks (FCN). The dataset contains 135,974 CT images, in which 33,391 images labeled as bleed, every CNN/FCN approaches were individually trained on image data preprocessed by utilizing two dissimilar level/width settings. This method was used to find out whether it is bleeding or not. The experimental results shows the accuracy is 97% by increasing the sensitivity as 96%, precision was 80.19%, recall was 82.15%. In this error rate was increased.

Weber et al.[32] have presented an effectiveness of head computed tomography scans before outpatient record for low-risk mild traumatic brain injury. Neurosurgeons were regularly built with traumatic brain injuries resultant at intracranial hemorrhage. The aim of the presented work was to evaluate the practice pattern and medical utility of routine outpatient head CT scans using mild traumatic brain injuries. The dataset contains 49 patients for the study of the head CT Brain Injury. From that, 21 patients were detected as subdural hematoma (SDH), seven patients were detected as expanded hemorrhage on outpatient imaging, remaining images were detected as traumatic brain injury and in the critical stage, but the computational time was increased.

3 | PROPOSED METHOD FOR DETECTING AND CATEGORIZING OF ACUTE ICH SUBTYPES USING A MULTILAYER DENSENET-RESNET ARCHITECTURE WITH IRF CLASSIFIER

Figure 1 shows the block diagram for detecting and categorizing of acute intracranial hemorrhage (ICH) subtypes using a multilayer DenseNet-ResNet architecture with IRF classifier. In this the brain CT imageries are taken through the physionet repository publicly dataset. The imageries are preprocessed to eliminate the unnecessary noises.

After that, the image features are extracted by using multilayer densely connected convolutional network (DenseNet) combined with residual network (ResNet) architecture with multiple convolutional layers. Then the sub types of ICH are subdural hemorrhage, epidural hemorrhage, intracerebral hemorrhage, subarachnoid hemorrhage, intraventricular hemorrhage are classified by using IRF classifier with high accuracy.

3.1 | Image acquisition

The CT imageries are gathered from the physionet repository publicly available ICH CT image dataset. The images are gathered from 82 CT scan machines. In this, the samples are detected from the patients age is in-between 27.8 and 19.5. In which, 46 cases are male, and 36 cases are female.

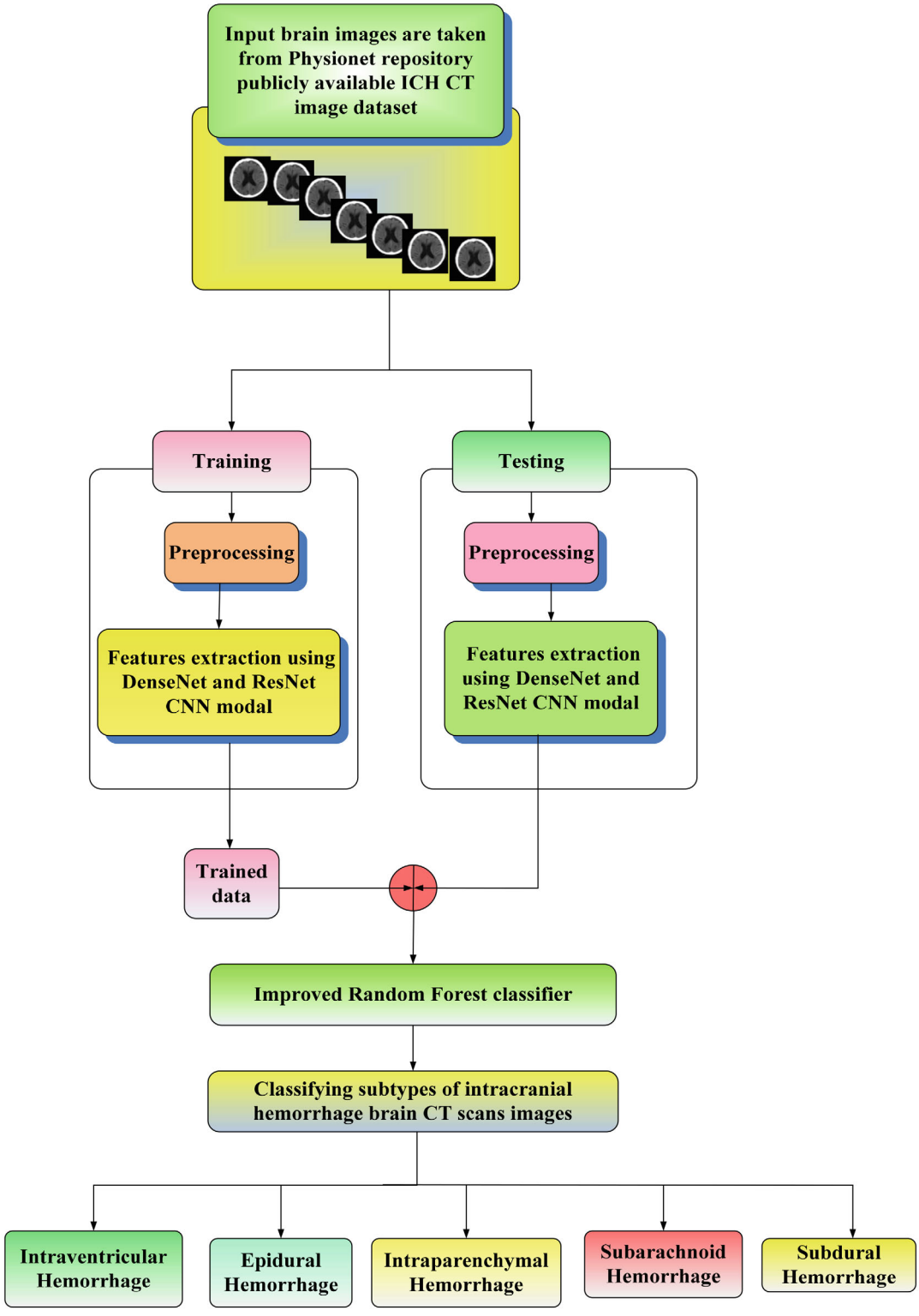

FIGURE 1 Block diagram proposed method

3.2 | Preprocessing

This is employed to eliminate the noises and the skull area of the CT images. Here, 2D Gaussian filters are taken to eliminate the noises. Before the image is given to the feature extracting convolutional models, the image smoothening is required. The equation of Gaussian filter is,

$$S_{g1d}(a) = \frac{1}{\sqrt{2\pi\sigma}} e^{-\left(\frac{a^2}{2\sigma^2}\right)}. \tag{1}$$

The above Equation (1) displays 1-dimensional Gaussian filter, here S_{g1d} implies i-dimensional Gaussian filter, σ implies sigma function for standard deviation at the Gaussian filter, a implies Cartesian co-ordinates. Then the 2-dimensional Gaussian equation is given in Equation (2)

$$S_{g2d}(a,b) = \frac{1}{\sqrt{2\pi\sigma}} e^{-\left(\frac{a^2+b^2}{2\sigma^2}\right)}, \tag{2}$$

where a, b represents the Cartesian co-ordinates, S_{g2d} indicates i-dimensional Gaussian filter, σ indicates sigma function for standard deviation at the Gaussian filter. The images are inserted in the type of matrix functions and the values are in-between 0 to 255 (8 bits). Then the binary functions are denoted in the form of 0, 1 with base 2. The noises are removed from the image and the images are smoothened. Then the features are removed using multilayer DenseNet-ResNet model.

3.3 | Feature extraction using combined ResNet and DenseNet model

Here, the most relevant features from region of interest (ROI) CT image are extracted using ResNet-DenseNet model. The image features are extracted to avert the over fitting problems while the process of classification. By this, it can identify what type of hemorrhages is affected and it is classify the images with great accuracy. Figure 2 shows the multilayer DenseNet-ResNet architecture. Then the parameter explanations of the multilayer DenseNet-ResNet architecture is given below,

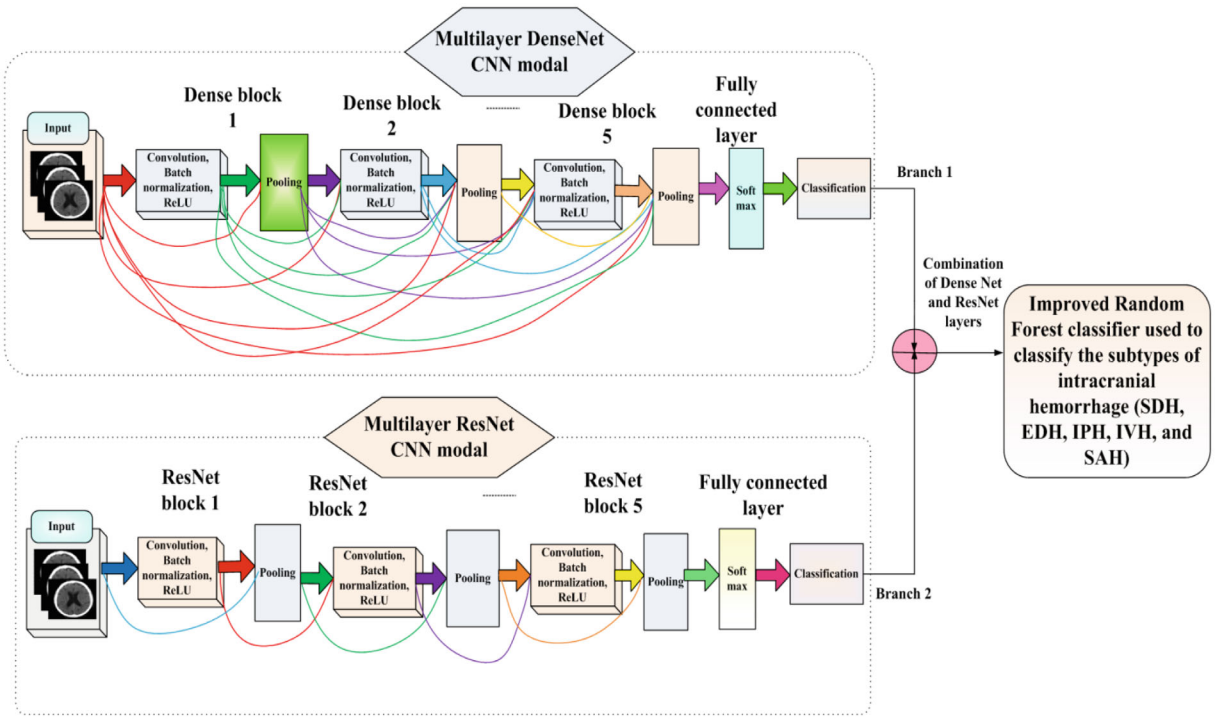

FIGURE 2 Multilayer DenseNet-ResNet architecture

3.3.1 | DenseNet model

DenseNet model is the one type of CNN architecture. The main function of the DenseNet model is the layers are connected in dense manner. It is the process of every layer in the network is directly linked to the all the blocks in the architecture as shown in Figure 2. Due to these properties of the dense layers, the image features are extracted and can be reused and gives strengthen to the feature transmission. Let us consider the densely connected layers as D_k and the output of the network is defined as the a_{k-1} with the layer $k-1$th, $D_k(a)$ represents the series of connections with one layer to the another, then the output kth layer with the a_k is formulated in Equation (3)

$$a_k = D_k\left([a_0, a_1, \ldots, a_{k-1}]\right), \tag{3}$$

where [.] is represented as the concatenation operation. Assume that the every functions in the D_k will generates the L features, at similar time of feature maps at kth layer is changed as $l_0 + l \times (k-1)$, where l_0 is denoted as the number of channels present in the input layer. Here the parameter l is growth rate and it will maintain the number of parameters in the architecture. The main features of the DenseNet are that it consists of less number of parameters when comparing with the other network and it does not use the learning redundant features.

3.4 | ResNet model

In this the ResNet is defined as the residual neural network (ResNet), which consists of residual learning features as shown in Figure 2 and it is formulated in Equation (4)

$$b = R\left(a, \left\{V_j\right\}\right) + a, \tag{4}$$

where a and b is represented as the input and the output layers in the network, V_j is represented as the weight in the weight matrix, and R is represented as the residual mapping functions in the learning process. Then the residual mapping functions are given in Equations (5) and (6).

$$R_{fm} = V_2 r\left(V_1 a + y_1\right) + y_2, \tag{5}$$

$$r(a) = \max(0, a), \tag{6}$$

where r is represented as the rectified linear unit in the activation functions, V_1, V_2, y_1, y_2 is represented as the weights and the bias in the first and the second layer.

In the proposed framework, a combined architecture formed by combining Res Net using DenseNet is utilized to extract the most critical and important features from the CT image. In this, the combined feature extraction framework utilizes multiple convolutional layers for training the input parameters.

The deployment of large number of convolutional layers can increase the training errors as well as degrade the classification accuracy. These limitations can be solved by employing a combined (ResNet-DenseNet) framework. The combined feature extraction framework uses multiple convolutional layers to learn the input and output parameters. Also, the combination of ResNet with DenseNet improves the training speed and detection accuracy of the proposed deep learning based feature extraction framework.

The ResNet-DenseNet unit is composed of various convolutional layers with ReLU (rectified linear unit) activation function.

In this study, the ResNet model establishes some skip connections between the front and back layers during training process to carry out back-propagation of the gradient. The process of back-propagation helps to achieve better training in the deep convolutional neural network and enables continuous transmission of information.

During training process, the area that is too small will be ignored since the resolutions of the convolutional layer are getting degraded. Therefore to protect the characteristics of small area or low dimension, in the proposed study a dense convolutional network called DenseNet is employed. The DenseNet connects an individual layer with other layers in the network in a feed-forward manner. Here, the dense layer is subsequent to transition layer. Transition layer is composed of 1×1 convolutional kernel. The count of channels in the transition layer is represented as $4k$, where the parameter k represents that growth rate. Here, $k = 4$ implies output feature image obtained from every layer contains dimension of 4. Also, the DenseNet model improves the feature reuse on one level.

In the combined ResNet-DenseNet model, the feature maps from the entire earlier layers is fed as input to each layers and the feature maps of its own is fed as input to the entire next layers. The combined feature extraction framework improves better propagation of features and enhances feature reuse strategy. Therefore, the low-dimensional features can also be identified effectively with the help of ResNet-DenseNet model.

The residuals in the ResNet-DenseNet model deepen the training process and do not eliminate even the low-dimensional features that are also necessary for the prediction process.

From this the features of the brain CT images are extracted and combination of two multilayer.

Assume the network consists of L convolutional layers, in which each layer implements a nonlinear transform function of $H_i(\cdot)$. Here, the parameter i denotes the ith layer that obtains the feature maps $u_0, u_1, \ldots, u_{i-1}$ as input from all the previous layers. Thus, the corresponding feature map at ith layer is expressed in Equation (7)

$$u_i = H_i([u_0, u_1, \ldots, u_{i-1}]), \tag{7}$$

In the above expression, the term $[u_0, u_1, \ldots, u_{i-1}]$ defines the feature maps obtaining in cascade manner. Also, the term $H_i(\cdot)$ denotes the nonlinear transformation function of two consecutive processes: ReLU activation function and $3 * 3$ convolution (Conv).

The output at cth convolutional layer is expressed in Equation (8)

$$V_{d,c} = H\left\{\left[V_{d-1}, V_{d,1}, \ldots, V_{d,c-1}\right]\right., \tag{8}$$

where the parameters V_{d-1} and V_d defines the input and output of dth unit, the number of feature maps is represented as F_0.

The number of feature maps at end unit is controlled for better feature extraction. This is done by 1×1 convolution in the model. It is expressed in Equation (9)

$$V_{d,LV} = H^d{}_{LVV}\left\{\left[V_{d-1}, V_{d,1}, \ldots \ldots, V_{d,c}\right]\right., \tag{9}$$

where, the term $H^d{}_{LVV}$ indicates 1×1 convolution.

Finally, the output from combined ResNet + DenseNet unit is expressed in Equation (10)

$$V_d = V_{d-1} + V_{d,LV}. \tag{10}$$

In the proposed feature extraction framework, a total of three layers of dense blocks are used that includes $3\,BN + ReLU + Conv(3 * 3)$ layer structures.

The statistical features are extracted with the help of ResNet-DenseNet model methods. Here, ResNet-DenseNet model is occur (a, b) components. It is scaled with pixel and its intensity is expressed as a with the relation of other pixel b and the distance is exhibited as c. The features are extracted in sampling circular form around the central pixels at uniform or nonuniform patterns. The radiomic features are categorized as mean, variance, entropy, and energy.

Here, the four features are extracted: mean variance, entropy, and energy. The mean value is defined as the ROI average mean pixel value, also this is applied to indicate the image brightness. Mean is expressed as,

$$M(I_n) = \frac{1}{e_i \times e_j}\sum_{X=1}^{e_i}\sum_{Y=1}^{e_j} O(i,j), \tag{11}$$

where i, j indicates co-ordinates of input image pixels along the center of images local region, e_i, e_j denotes neighbor pixels gray intensity values, $O(i, j)$ is represented as the sampling center of imagery pixel. Energy is defined as the values through the arithmetic mean. The energy is expressed as,

$$Eng = \sum_{j=1}^{X_i}\left(\left[i, j\left(e_{(i)}e_{(j)}\right)\right] - mean\right)^2, \tag{12}$$

where i, j is represented as the co-ordinates of input image pixels along the center of images local region, e_i, e_j denotes neighbor pixels gray intensity values. Entropy is determined as the cube of the variance of the image among two different variables functions that is shown in Equation (13)

$$En = \frac{1}{\text{variance}^3}\sum_{j=1}^{X_i}\left(\left[\left(e_{(i)}, e_{(j)}\right)\right] - mean\right)^3. \tag{13}$$

The variance is the scaling of distance amid the two or more image features that need to be extracted,

$$V = \frac{1}{e_i \times e_j}\sum_{i=1}^{e_i}\sum_{j=1}^{e_j}(e(i,j) - mean)^2. \tag{14}$$

After extracting these features, it is given to the IRF classifier for classifying acute intracranial hemorrhage (ICH) subtype as EDH, SDH, SAH, ICH, and IVH.

Then the images are classified using IRF classifier. The features are extracted to avoid over fitting problem during classification and this method increases the speed and reduces the computational time and also the accuracy is increased.

3.5 | Subtypes of intracranial hemorrhage images are classified using improved RF classifier

IRF classifier is utilized to classify the sub types of intracranial hemorrhage on the basis of EDH, SAH, SDH, ICH, IVH with high accuracy.

RF classifier generates m decision trees, $\{R_j(V)\}$ $(i = 1, 2, \ldots m)$, where C is represented as feature extracted through the length $n(n = 386)$. Let the feature set V_i contains the feature vectors $V_1, V_2, \ldots, V_m$, where, $i = 1, 2, \ldots, m$. Here, the feature significance score $F_{IRF}(V)$ implies every feature is evaluated based on how often it is utilized to distribute the training data across the entire tree.

The feature significance score is given as follows,

The final result is given as $F_{IRF}(V)$, it is determined by selecting the decision trees and the equation is given Equation (15)

$$F_{IRF}(C) = \frac{1}{L}\sum_{j=1}^{L} R_j(V). \tag{15}$$

The main purpose of the IRF classifier is to select the feature extracted values in random process, the dimension reduction values varies with time when various features are extracted, this may increases complex to the classifier. To recover that high efficiency of classification accuracy, the input features $F_{IRF}(V)$ with n components are selected. To estimate the significant point as SR_i with the ith component of $F_{IRF}(V)$, the input feature is referred to be V_i. The significance of V_i is denoted as the point SR_i, then the classification output at ith data point is expressed in Equation (16),

$$SR_i = \frac{1}{L_i}\sum_{nz_i} Gain\,(V_i, n)\,, \tag{16}$$

where Z_i is represented as the node set with L_i, $Gain\,(V_i, n)$ is represented as the information gained and the gain is calculated in Equation (17),

$$Gain\,(V_i, n) = GINI\,(V_i, n) - qkGINI\left(V_i, n^K\right) - qTGINI\left(V_i, n^T\right). \tag{17}$$

The above Equation 19 is known as the classification equation. Where n^K and n^T is represented as the right and left child nodes of n, $qk\left(qk = M\left(n^k\right) / \left(M\left(n^k\right) + M\left(n^T\right)\right)\right)$, and $qT\left(qT = M\left(n^T\right) / \left(M\left(n^T\right) + M\left(n^T\right)\right)\right)$ is represented as the proportions of right and left child nodes. The loss function for classifying acute ICH subtypes $GINI\,(V_i, n)$ is given in Equation (18),

$$GINI\,(V_i, n) = 1 - \sum_{n=1}^{N} q_n^{V^2}, \tag{18}$$

where $q_n^{V^2}$ is represented as the proportion of the class-c with the node n and $v = 6$. From this the output images are classified into six classes with higher accuracy by lessening computational time. In the above expression, the parameter V represents the loss function that estimates how well the proposed classification model is predictive.

3.6 | Computational time complexity

The computational time complexity is calculated in the random forest classifier. Consider n is denoted as the dimension of the features with the total number of samples and L specifies the decision trees. The computational time is given in Equation (19),

$$IRF_{cc} = C(L * n * m * \log(m)). \tag{19}$$

Then the feature extracted classifications of the IRF computational complexity equation is given in Equation (20),

$$IRF_{cc} = C(L * n * m * \log(m)) + C\,(L_i * n * m) + C(n\log(n)) \approx C(L * n * m * \log(m)). \tag{20}$$

The above equation represents the computational time complexity equation with the feature dimension of (n) and it is equal to the number of samples square (n). When likened to n and m, L represents very small, so the L value is neglected. Then the running time of this method is reduced and generated high dimensional data with high accuracy.

4 | RESULT WITH DISCUSSION

Here, the simulation results with discussion are described. The detection and categorization of acute intracranial hemorrhage (ICH) subtype's using a multilayer DenseNet-ResNet architecture with IRF classifier is proposed in this article. The MATLAB simulations are activated PC through Intel Core i5, 8GB RAM, 2.50 GHz CPU, Windows 7. The proposed method is carried out in MATLAB, its performance is likened with existing methods. Moreover, performance metrics, like computational time, recall, F-score, precision, specificity, accuracy are analyzed to validate the efficiency of the proposed method.

4.1 | Dataset description

The CT imageries are gathered from the Physionet repository publicly available[20] ICH CT image dataset. Here, the size of each CT image is 650×650 pixels. Here, 82 CT scans dataset were gathered, in which, 46 are male patients and 36 are female patients including 36 scans for patients diagnosed with intracranial hemorrhage like intraventricular (IV), intraparenchymal (IP), subarachnoid (SA), epidural (ED), and subdural (SD). Each CT scan for each patient involves 30 slices with 5 mm slice-thickness. In the proposed study, 80% of CT slices are employed for training and remaining 20% of CT slices are used as testing set. The feature dimension of input CT image is $168 \times 299 \times 3$ pixels, ROI extraction is $147 \times 87 \times 3$ pixels, SAH is $150 \times 84 \times 3$ pixels, EDH is $150 \times 76 \times 3$ pixels, SDH is $153 \times 72 \times 3$ pixels, IVH is $154 \times 84 \times 3$ pixels, and IPH is $160 \times 83 \times 3$ pixels.

4.2 | Performance metrics

The confusion matrix is used to calculate the precision, F-Measure, accuracy, recall, specificity, and error rate. The values of true negative (TN), true positive (TP), false negative (FN), and false positive (FP) have been essential to scale the confusion matrix.

- TP (TPA): intracranial hemorrhage brain CT imageries are categorized as normal into normal.
- TN (TNN): intracranial hemorrhage brain CT imageries are categorized as normal into abnormal.
- FP ($FPAN$): intracranial hemorrhage brain CT imageries are categorized as abnormal into normal.
- FN ($FNNA$): intracranial hemorrhage brain CT imageries are categorized as abnormal into abnormal.

4.2.1 | Precision

The precision is known as true positive predictive values,

$$\text{Precesion value} = \frac{TPA}{TPA + FPAN} \times 100\%. \tag{21}$$

4.2.2 | F-score

F score is computed by,

$$\text{F-Score value} = \frac{2 \times TPA}{2 \times TPA + FPAN + FNNA} \times 100\%. \tag{22}$$

4.2.3 | Accuracy

Accuracy values can be computed by the given Equation (23)

$$\text{Accuracy} = \frac{TPA + TNN}{TPA + TNN + FPAN + FPNN} \times 100\%. \tag{23}$$

4.2.4 | Sensitivity

Sensitivity is named as true positive rate or recall,

$$\text{Sensitivity}\,(TPR) = \frac{TPP}{TPP + FNNA} \times 100\%. \tag{24}$$

4.2.5 | Specificity

Specificity is known as true negative rate (TNR),

$$\text{Specificity}\,(TNR) = \frac{TNN}{TNN + FPAN} \times 100\%. \tag{25}$$

4.3 | Comparison of performance analysis utilizing various models for subtypes of Intracranial Hemorrhage (IPH, IVH, SDH, EDH, SAH) under brain CT scans

Figure 3 shows the detection and categorization of acute intracranial hemorrhage (ICH) subtypes using a brain CT images. The brain CT imageries are taken from the Physionet repository publicly dataset. After that, the imageries are preprocessed to take away the unnecessary noises. The image features are extracted by utilizing multilayer DenseNet combined with ResNet architecture with multiple convolutional layers. Then the sub types of ICH are intracerebral hemorrhage, intraventricular hemorrhage, epidural hemorrhage, subdural hemorrhage, subarachnoid hemorrhage is classified by using IRF classifier with high accuracy.

4.3.1 | Simulation phase: 1

Tables 1–7 shows the simulation results obtained from the proposed acute ICH detection and classification model for training–testing % are illustrated below in a tabular form. Here, the proposed ICH-DC-ResNet-DenseNet-IRF method compared with existing deep learning algorithm for

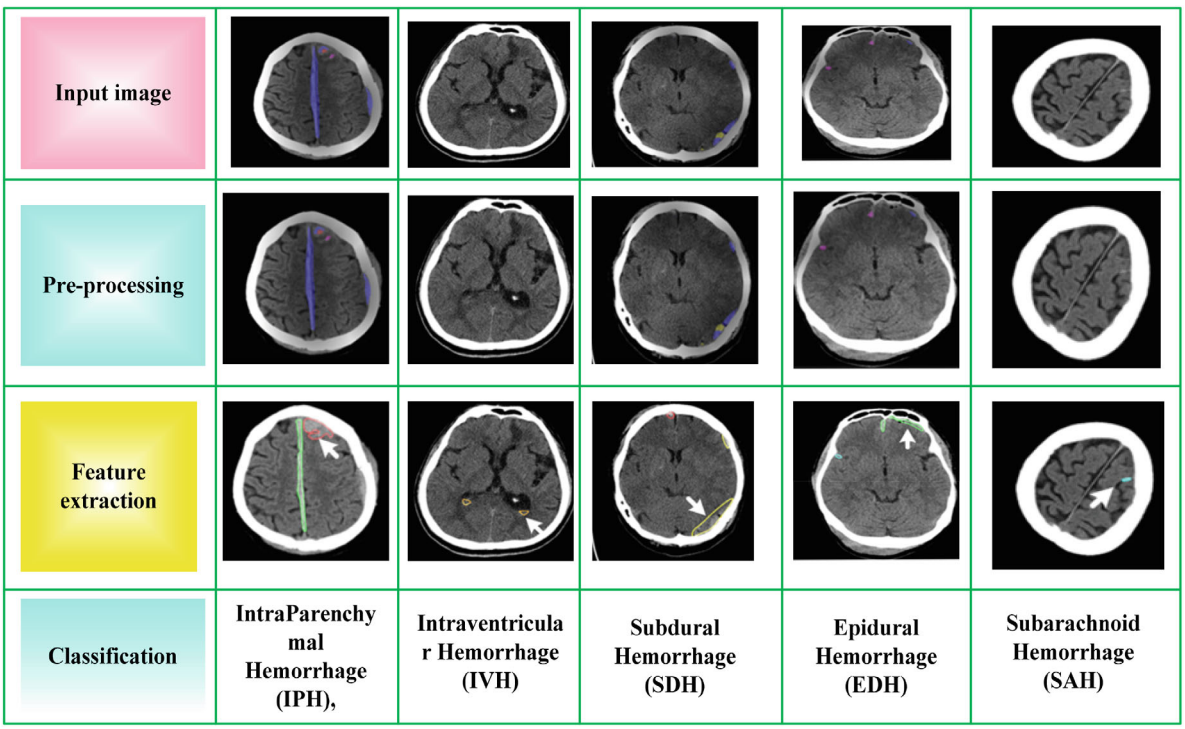

FIGURE 3 Automated detection and classification subtypes of intracranial hemorrhage (IPH, IVH, SDH, EDH, SAH) using brain CT scans

TABLE 1 Performance of accuracy

Methods and types of acute ICH	SDH	EDH	IPH	IVH	SAH
ICH-DC-CNN	78.65	69.08	72.97	73.97	69.08
ICH-DC-2D-CNN	74.98	71.98	69.65	74.97	74.86
ICH-DC-FSVM	83.76	79.05	74.97	76.86	68.95
ICH-DC-CNN-FCNs	74.86	85.89	75.74	67.04	84.87
ICH-DC-ResNet-DenseNet-IRF (Proposed)	99.53	98.75	98.09	99.8	99.46

TABLE 2 Performance of specificity

Methods and types of acute ICH	SDH	EDH	IPH	IVH	SAH
ICH-DC-CNN	77.54	62.98	69.87	64.76	76.43
ICH-DC-2D-CNN	74.98	71.98	69.65	74.97	74.86
ICH-DC-FSVM	59.87	65.87	75.87	60.99	74.86
ICH-DC-CNN-FCNs	62.86	73.86	56.98	63.87	74.87
ICH-DC-ResNet-DenseNet-IRF (Proposed)	93.86	90.53	91.75	93.86	95.87

TABLE 3 Sensitivity performance

Methods and types of acute ICH	SDH	EDH	IPH	IVH	SAH
ICH-DC-CNN	61.86%	66.95%	49.87%	54.65%	75.76%
ICH-DC-2D-CNN	51.43	61.76	75.86	69.98	59.08
ICH-DC-FSVM	66.54	54.86	66.86	61.34	52.76
ICH-DC-CNN-FCNs	69.07	53.44	72.6	62.76	71.75
ICH-DC-ResNet-DenseNet-IRF (Proposed)	91.86	93.87	90.45	93.97	92.33

TABLE 4 Precision performance

Methods and types of acute ICH	SDH	EDH	IPH	IVH	SAH
ICH-DC-CNN	54.64	73.65	59.08	74.75	69.54
ICH-DC-2D-CNN	55.86	63.75	73.75	65.43	60.54
ICH-DC-FSVM	74.64	66.96	70.64	64.75	69.07
ICH-DC-CNN-FCNs	69.43%	74.34%	69.66%	65.86%	73.54%
ICH-DC-ResNet-DenseNet-IRF (Proposed)	96.44	95.61	94.43	97.96	94.66

TABLE 5 F-Measure performance

Methods and types of acute ICH	SDH	EDH	IPH	IVH	SAH
ICH-DC-CNN	66.95	59.05	75.45	75.86	64.86
ICH-DC-2D-CNN	73.74	76.00	73.83	63.65	59.94
ICH-DC-FSVM	49.03	66.93	68.92	59.03	75.04
ICH-DC-CNN-FCNs	49.07	74.86	52.66	62.74	58.64
ICH-DC-ResNet-DenseNet-IRF (Proposed)	95.45	94.86	92.64	93.66	90.65

TABLE 6 Recall performance

Methods and types of acute ICH	SDH	EDH	IPH	IVH	SAH
ICH-DC-CNN	56.97	63.93	65.92	63.05	53.92
ICH-DC-2D-CNN	77.97	67.86	59.02	59.03	60.93
ICH-DC-FSVM	49.08	72.86	71.92	71.93	65.93
ICH-DC-CNN-FCNs	77.66	77.97	58.09	73.03	62.12
ICH-DC-ResNet-DenseNet-IRF (Proposed)	92.03	91.92	93.92	92.93	89.02

TABLE 7 Computational time (s) performance

Methods and types of acute ICH	SDH	EDH	IPH	IVH	SAH
ICH-DC-CNN	61.86	66.95	49.87	54.65	75.76
ICH-DC-2D-CNN	51.43	61.76	75.86	69.98	59.08
ICH-DC-FSVM	66.54	54.86	66.86	61.34	52.76
ICH-DC-CNN-FCNs	69.07	53.44	72.6	62.76	71.75
ICH-DC-ResNet-DenseNet-IRF (proposed)	19.71	29.08	24.86	20.54	32.83

automatic detection with classification of acute intracranial hemorrhages in head CT scans (ICH-DC-2D-CNN),[33] fusion-based deep learning along nature-inspired algorithm for the diagnosis of intracerebral hemorrhage (ICH-DC-FSVM)[34] and detection of intracranial hemorrhage on CT scan images utilizing convolutional neural network (ICH-DC-CNN),[35] ICH-DC-CNN-FCNs[31] methods, respectively.

Table 1 depicts the performance of accuracy of the proposed method ICH-DC-ResNet-DenseNet-IRF compared with existing ICH-DC-2D-CNN, ICH-DC-FSVM ICH-DC-CNN, and ICH-DC-CNN-FCNs methods under classifying the subtypes of acute ICH, such as EDH, SDH, SAH, ICH, and IVH. For epidural hemorrhage (EDH), the proposed ICH-DC-ResNet-DenseNet-IRF method provides 30.66%, 34.76%, 26.86%, and 22.5% higher accuracy than the existing ICH-DC-2D-CNN, ICH-DC-FSVM ICH-DC-CNN, and ICH-DC-CNN-FCNs methods. For subdural hemorrhage (SDH), the proposed ICH-DC-ResNet-DenseNet-IRF method provides 22.5%, 27.27%, 36.86%, and 8.88% higher accuracy than the existing methods. For subarachnoid hemorrhage (SAH), the proposed ICH-DC-ResNet-DenseNet-IRF method provides 16.47%, 34.54%, and 32% higher accuracy than the existing methods. For intracerebral hemorrhage (ICH), the proposed ICH-DC-ResNet-DenseNet-IRF method provides 11.76%, 47.12%, 22.08% and 18.75% higher accuracy than the existing methods. For Intraventricular Hemorrhage (IVH), the proposed ICH-DC-ResNet-DenseNet-IRF method provides 12.5%, 27.92%, 21.86%, and 23.75% higher accuracy than the existing methods, respectively.

Table 2 depicts the performance of the specificity for proposed ICH-DC-ResNet-DenseNet-IRF method compared with the existing ICH-DC-2D-CNN, ICH-DC-FSVM ICH-DC-CNN, and ICH-DC-CNN-FCNs methods under classifying the subtypes of acute ICH such as EDH, SDH, SAH, ICH and IVH. For epidural hemorrhage (EDH), the proposed ICH-DC-ResNet-DenseNet-IRF method provides 26.43%, 37.87%, 32.54%, and 22.97% better Specificity than the existing ICH-DC-2D-CNN, ICH-DC-FSVM ICH-DC-CNN, and ICH-DC-CNN-FCNs methods. For subdural hemorrhage (SDH), the proposed ICH-DC-ResNet-DenseNet-IRF method provides 32.76%, 16.87%, 27.87%, and 14.86% better specificity than the existing ICH-DC-2D-CNN, ICH-DC-FSVM ICH-DC-CNN, and ICH-DC-CNN-FCNs methods. For subarachnoid hemorrhage (SAH), the proposed ICH-DC-ResNet-DenseNet-IRF method provides 21.87%, 36.86%, 41.87%, and 26.87% higher specificity than the existing ICH-DC-2D-CNN, ICH-DC-FSVM ICH-DC-CNN, and ICH-DC-CNN-FCNs methods. For intracerebral hemorrhage (ICH), the proposed ICH-DC-ResNet-DenseNet-IRF method provides 32.76%, 21.75%, 21.76%, 29.05% better specificity than the existing ICH-DC-2D-CNN, ICH-DC-FSVM ICH-DC-CNN, and ICH-DC-CNN-FCNs methods. For intraventricular hemorrhage (IVH), the ICH-DC-ResNet-DenseNet-IRF method provides 21.76%, 31.75%, 11.86%, and 31.86% higher specificity than the existing ICH-DC-2D-CNN, ICH-DC-FSVM ICH-DC-CNN, and ICH-DC-CNN-FCNs methods, respectively.

Table 3 depicts the performance of the sensitivity for proposed ICH-DC-ResNet-DenseNet-IRF method compared with the existing ICH-DC-2D-CNN, ICH-DC-FSVM ICH-DC-CNN, and ICH-DC-CNN-FCNs methods under classifying the subtypes of acute ICH, such as EDH, SDH, SAH, ICH, and IVH. For epidural hemorrhage (EDH), the proposed ICH-DC-ResNet-DenseNet-IRF method provides 32.86%, 41.76%, 32.76%, and 22.75% higher sensitivity than the existing ICH-DC-2D-CNN, ICH-DC-FSVM ICH-DC-CNN, and ICH-DC-CNN-FCNs methods. For subdural hemorrhage (SDH), the proposed ICH-DC-ResNet-DenseNet-IRF method provides 26.86%, 21.76%, 33.87%, and 20.86% better sensitivity than the existing ICH-DC-2D-CNN, ICH-DC-FSVM ICH-DC-CNN, and ICH-DC-CNN-FCNs methods. For subarachnoid hemorrhage (SAH), the proposed ICH-DC-ResNet-DenseNet-IRF method provides 43.86%, 21.86%, 31.44%, and 28.97% higher Sensitivity than the existing methods. For Intracerebral Hemorrhage (ICH), the proposed ICH-DC-ResNet-DenseNet-IRF method provides 32.87%, 38.87%, 25.86% and 22.63% higher sensitivity

than the existing methods. For intraventricular hemorrhage (IVH), the proposed ICH-DC-ResNet-DenseNet-IRF method provides 31.76%, 27.77%, 31.75%, and 29.08% higher sensitivity than the existing ICH-DC-2D-CNN, ICH-DC-FSVM ICH-DC-CNN, and ICH-DC-CNN-FCNs methods, respectively.

Table 4 depicts the performance of Precision for the proposed ICH-DC-ResNet-DenseNet-IRF method compared with the existing ICH-DC-2D-CNN, ICH-DC-FSVM ICH-DC-CNN, and ICH-DC-CNN-FCNs methods under classifying the subtypes of acute ICH, such as EDH, SDH, SAH, ICH, and IVH. For epidural hemorrhage (EDH), the proposed ICH-DC-ResNet-DenseNet-IRF method provides 25.87%, 27.86%, 31.64%, and 26.86% better Precision than the existing ICH-DC-2D-CNN, ICH-DC-FSVM ICH-DC-CNN, and ICH-DC-CNN-FCNs methods, respectively. For subdural hemorrhage (SDH), the proposed ICH-DC-ResNet-DenseNet-IRF method provides 36.75%, 31.77%, 26.86%, and 31.97% higher precision than the existing methods. For subarachnoid hemorrhage (SAH), the proposed ICH-DC-ResNet-DenseNet-IRF method provides 31.87%, 28.97%, 35.97%, and 27.55% higher precision than the existing methods. For intracerebral hemorrhage (ICH), the proposed ICH-DC-ResNet-DenseNet-IRF method provides 32.77%, 17.86%, 26.86%, and 31.86% better precision than the existing ICH-DC-2D-CNN, ICH-DC-FSVM ICH-DC-CNN, and ICH-DC-CNN-FCNs methods. For intraventricular hemorrhage (IVH), the proposed ICH-DC-ResNet-DenseNet-IRF method provides 32.86%, 26.46%, 27.86%, and 32.86% higher precision than the existing ICH-DC-2D-CNN, ICH-DC-FSVM ICH-DC-CNN, and ICH-DC-CNN-FCNs methods, respectively.

Table 5 depicts the performance of F-Measure for the proposed ICH-DC-ResNet-DenseNet-IRF method compared with the existing ICH-DC-2D-CNN, ICH-DC-FSVM ICH-DC-CNN, and ICH-DC-CNN-FCNs methods under classifying the subtypes of acute ICH, such as EDH, SDH, SAH, ICH, and IVH. For epidural hemorrhage (EDH), the proposed ICH-DC-ResNet-DenseNet-IRF method provides 21.84%, 31.76%, 30.97%, and 26.85% higher F-Measure than the existing ICH-DC-2D-CNN, ICH-DC-FSVM ICH-DC-CNN, and ICH-DC-CNN-FCNs methods. For subdural hemorrhage (SDH), the proposed ICH-DC-ResNet-DenseNet-IRF method provides 31.76%, 25.97%, 20.93%, and 21.75% higher F-Measure than the existing methods. For subarachnoid hemorrhage (SAH), the proposed ICH-DC-ResNet-DenseNet-IRF method provides 32.86%, 16.97%, 26.88%, and 24.55% higher F-Measure than the existing methods. For intracerebral hemorrhage (ICH), the proposed ICH-DC-ResNet-DenseNet-IRF method provides 21.97%, 33.86%, 27.97%, and 41.87% higher F-Measure than the existing methods. For intraventricular hemorrhage (IVH), the proposed ICH-DC-ResNet-DenseNet-IRF method provides 36.97%, 24.97%, 32.97%, and 21.87% higher F-Measure than the existing methods, respectively.

Table 6 depicts the performance of Recall of the proposed ICH-DC-ResNet-DenseNet-IRF method compared with existing ICH-DC-2D-CNN, ICH-DC-FSVM ICH-DC-CNN, and ICH-DC-CNN-FCNs methods under classifying the subtypes of acute ICH such as EDH, SDH, SAH, ICH, and IVH. For epidural hemorrhage (EDH), the proposed ICH-DC-ResNet-DenseNet-IRF method provides 23.64%, 27.97%, 27.83%, and 16.86% better

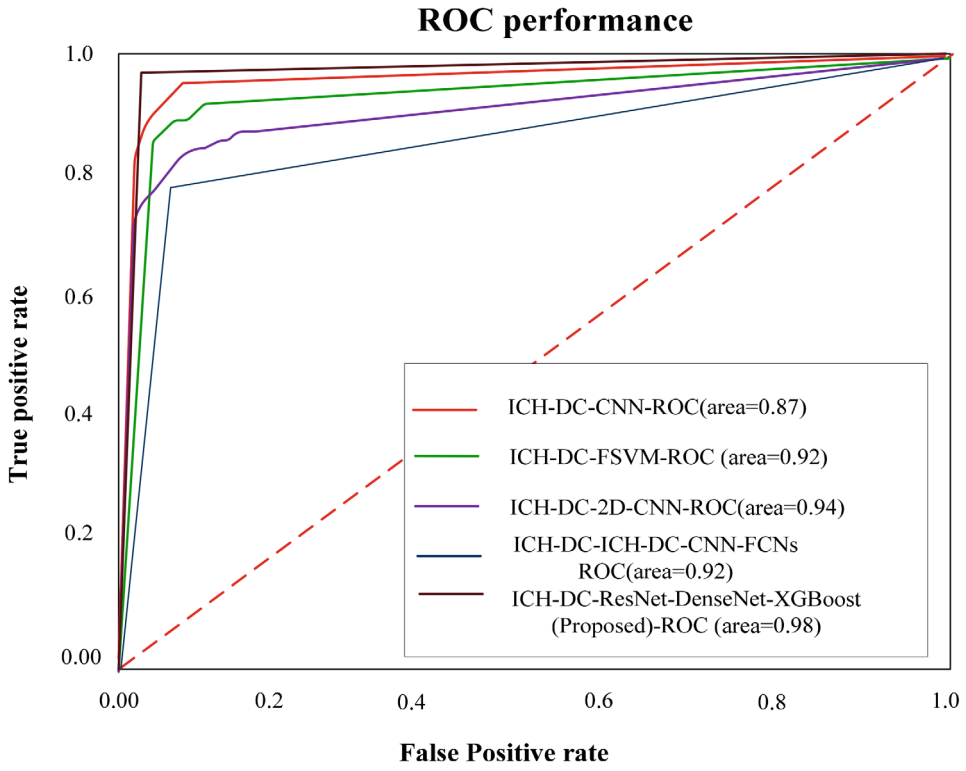

FIGURE 4 ROC curve performance

Recall than the existing ICH-DC-2D-CNN, ICH-DC-FSVM ICH-DC-CNN, and ICH-DC-CNN-FCNs methods. For subdural hemorrhage (SDH), the proposed ICH-DC-ResNet-DenseNet-IRF method provides 17.87%, 32.86%, 32.86%, and 34.97% higher recall than the existing methods. For subarachnoid hemorrhage (SAH), the proposed ICH-DC-ResNet-DenseNet-IRF method provides 26.86%, 17.98%, 23.76%, and 25.97% higher recall than the existing methods. For intracerebral hemorrhage (ICH), the proposed ICH-DC-ResNet-DenseNet-IRF method provides 21.87%, 32.86%, 23.98%, and 31.87% higher recall than the existing methods. For intraventricular hemorrhage (IVH), the proposed ICH-DC-ResNet-DenseNet-IRF method provides 34.65%, 21.65%, 32.76%, and 21.01% higher recall than the existing methods, respectively.

Table 7 depicts the performance of computational time of the proposed ICH-DC-ResNet-DenseNet-IRF method compared with existing methods, such as ICH-DC-2D-CNN, ICH-DC-FSVM ICH-DC-CNN, and ICH-DC-CNN-FCNs under classifying the subtypes of acute ICH such as EDH, SDH, SAH, ICH, and IVH. For epidural hemorrhage (EDH), the proposed ICH-DC-ResNet-DenseNet-IRF method provides 16.87%, 31.86%, 31.86% and 28.97% lower computational time than the existing ICH-DC-2D-CNN, ICH-DC-FSVM ICH-DC-CNN, and ICH-DC-CNN-FCNs methods. For subdural hemorrhage (SDH), the proposed ICH-DC-ResNet-DenseNet-IRF method provides 31.75%, 17.87%, 26.437%, and 20.98% lower computational time than the existing methods. For subarachnoid hemorrhage (SAH), the proposed ICH-DC-ResNet-DenseNet-IRF method provides 32.32%, 42.86%, 32.87%, and 22.867% lower computational time than the existing methods. For intracerebral hemorrhage (ICH), the proposed ICH-DC-ResNet-DenseNet-IRF method provides 23.86%, 25.87%, 34.52%, and 32.76% lower computational time than the existing methods. For intraventricular hemorrhage (IVH), the proposed ICH-DC-ResNet-DenseNet-IRF method provides 32.64%, 22.75%, 31.65%, and 32.65% lower computational time than the existing methods, respectively.

Figure 4 portrays the ROC Curve of proposed ICH-DC-ResNet-DenseNet-IRF and existing as ICH-DC-2D-CNN, ICH-DC-FSVM, and ICH-DC-CNN methods, respectively. Here, the proposed ICH-DC-ResNet-DenseNet-IRF method provides 3.157%, 4.158%, 26.97%, and 2.098% higher AUC than the existing methods, like ICH-DC-2D-CNN, ICH-DC-FSVM ICH-DC-CNN, and ICH-DC-CNN-FCNs, respectively.

5 | CONCLUSION

In this article, the detection and categorization of acute intracranial hemorrhage subtypes using a multilayer DenseNet-ResNet architecture with IRF classifier is successfully implemented. The simulation is done in MATLAB site. The proposed multilayer-DenseNet-ResNet-IRF attains higher precision 23.86%, 26.86%, 33.75%, 16.87% compared with the existing methods, such as ICH-DC-2D-CNN, ICH-DC-FSVM and ICH-DC-CNN, and FCNs, respectively.

FUNDING INFORMATION

This research did not receive any specific grant from funding agencies in the public, commercial, or not-for-profit sectors.

DATA AVAILABILITY STATEMENT

Data sharing is not applicable to this article as no new data were created or analyzed in this study.

ORCID

Balraj M. Monica Jenefer https://orcid.org/0000-0002-5510-4160

REFERENCES

1. Xue M, Yong V. Neuroinflammation in intracerebral haemorrhage: immunotherapies with potential for translation. *Lancet Neurol*. 2020;19(12):1023-1032.
2. Shi K, Tian DC, Li ZG, Ducruet AF, Lawton MT, Shi FD. Global brain inflammation in stroke. *Lancet Neurol*. 2019;18(11):1058-1066.
3. Sturiale CL, Pignotti F, Giordano M, et al. Antithrombotic therapy and intracranial bleeding in subjects with sporadic brain arteriovenous malformations: preliminary results from a retrospective study. *Intern Emerg Med*. 2018;13(8):1227-1232.
4. de Melo Junior JO, Melo MA, Junior LA, et al. Therapeutic anticoagulation for venous thromboembolism after recent brain surgery: evaluating the risk of intracranial hemorrhage. *Clin Neurol Neurosurg*. 2020;197:106202.
5. Rashidi A, Lilla N, Skalej M, Sandalcioglu IE, Luchtmann M. Impact of acetylsalicylic acid in patients undergoing cerebral aneurysm surgery–should the neurosurgeon really worry about it?. *Neurosurg Rev*. 2021;25:1–0, 2898.
6. Shannon BC, Pruitt P, Borczuk P. The utility of computed tomography angiogram in patients with mild traumatic subarachnoid hemorrhage. *J Emerg Med*. 2021;61:456-465.
7. Murphy SJ, Werring DJ. Stroke: causes and clinical features. *Medicine*. 2020;48:561-566.
8. Lee SH. Symptoms and signs of hemorrhagic stroke. *InStroke Revisited: Hemorrhagic Stroke* 2018 (pp. 103-108). Springer.Click here to enter text.
9. Rajdev K, Siddiqui EM, Jadaun KS, Mehan S. Neuroprotective potential of solanesol in a combined model of intracerebral and intraventricular hemorrhage in rats. *IBRO Rep*. 2020;8:101-114.
10. Shajin FH, Rajesh P, Thilaha S. Bald eagle search optimization algorithm for cluster head selection with prolong lifetime in wireless sensor network. *J Soft Comput Eng Appl*. 2020;1(1):7.

11. Rajesh P, Shajin FH, Mouli Chandra B, Kommula BN. Diminishing energy consumption cost and optimal energy management of photovoltaic aided electric vehicle (PV-EV) by GFO-VITG approach. *Energy Sources A Recov Utiliz Environ Effects*. 2021;1-9. doi:10.1080/15567036.2021.1986606
12. Shajin FH, Rajesh P. FPGA realization of a reversible data hiding scheme for 5G MIMO-OFDM system by chaotic key generation-based paillier cryptography along with LDPC and its side channel estimation using machine learning technique. *J Circuits Syst Comput*. 2022;31(05):2250093.
13. Rajesh P, Shajin FH, Umasankar L. A novel control scheme for PV/WT/FC/battery to power quality enhancement in micro grid system: a hybrid technique. *Energy Sources A Recov Utiliz Environ Effects*. 2021;1-7. doi:10.1080/15567036.2021.1943068
14. Elgamal EA. Traumatic brain injury and disorders of intracranial pressure in children. *Clinical Child Neurology*. Springer; 2020;1001-1031.
15. Ollikainen JP, Janhunen HV, Tynkkynen JA, et al. The finnish prehospital stroke scale detects thrombectomy and thrombolysis candidates—A propensity score-matched study. *J Stroke Cerebrovasc Dis*. 2018;27(3):771-777.
16. Liu H, Sun X, Zou W, et al. Scalp acupuncture attenuates neurological deficits in a rat model of hemorrhagic stroke. *Complement Ther Med*. 2017;32:85-90.
17. Gautam A, Raman B. Automatic segmentation of intracerebral hemorrhage from brain CT images. *Machine Intelligence and Signal Analysis*. Springer; 2019;748:753-764.
18. Peng SJ, Lee CC, Wu HM, et al. Fully automated tissue segmentation of the prescription isodose region delineated through the gamma knife plan for cerebral arteriovenous malformation (AVM) using fuzzy C-means (FCM) clustering. *NeuroImage Clin*. 2019;21:101608.
19. Raghavendra U, Gudigar A, Vidhya V, et al. Novel and accurate non-linear index for the automated detection of haemorrhagic brain stroke using CT images. *Complex Intell Syst*. 2021;7(2):929-940.
20. Champagne AA, Wen Y, Selim M, et al. Quantitative susceptibility mapping for staging acute cerebral hemorrhages: comparing the conventional and multiecho complex Total field inversion magnetic resonance imaging MR methods. *J Magn Reson Imaging*. 2021;54:1843-1854.
21. Yuan Y, Qin W, Ibragimov B, et al. Densely connected neural network with unbalanced discriminant and category sensitive constraints for polyp recognition. *IEEE Trans Automat Sci Eng*. 2019;17(2):574-583.
22. Li Q, Jia W, Sun M, Hou S, Zheng Y. A novel green apple segmentation algorithm based on ensemble U-net under complex orchard environment. *Comput Electron Agric*. 2021;180:105900.
23. Yang B, Cao JM, Jiang DP, Lv JD. Facial expression recognition based on dual-feature fusion and improved random forest classifier. *Multimed Tools Appl*. 2018;77(16):20477-20499.
24. Anupama CS, Sivaram M, Lydia EL, Gupta D, Shankar K. Synergic deep learning model–based automated detection and classification of brain intracranial hemorrhage images in wearable networks. *Pers Ubiquit Comput*. 2020;1-0:1-10.
25. Faried A, Halim D, Widjaya IA, Badri RF, Sulaiman SF, Arifin MZ. Correlation between the skull base fracture and the incidence of intracranial hemorrhage in patients with traumatic brain injury. *Chin J Traumatol*. 2019;22(5):286-289.
26. Ye H, Gao F, Yin Y, et al. Precise diagnosis of intracranial hemorrhage and subtypes using a three-dimensional joint convolutional and recurrent neural network. *Eur Radiol*. 2019;29(11):6191-6201.
27. Prinz V, Manekeller L, Menk M, et al. Clinical management and outcome of adult patients with extracorporeal life support device–associated intracerebral hemorrhage—a neurocritical perspective and grading. *Neurosurg Rev*. 2021;1-0:2879-2888.
28. Rava RA, Seymour SE, LaQue ME, et al. Assessment of an artificial intelligence algorithm for detection of intracranial hemorrhage. *World Neurosurg*. 2021;150:e209-e217.
29. Kishan DM, Janardhan V. *Department of Information Technology, School of Engineering and Technology*. CMR University; 2020.
30. Thirunavukkarasu K, Gupta A, Abimannan S, Khan S. Intracranial hemorrhage detection using deep convolutional neural network. *Innovations in Computer Science and Engineering*. Springer; 2021:429-436.
31. Cho J, Park KS, Karki M, et al. Improving sensitivity on identification and delineation of intracranial hemorrhage lesion using cascaded deep learning models. *J Digit Imaging*. 2019;32(3):450-461.
32. Weber MW, Nie JZ, Watson VL, et al. Utility of head computed tomography scans before outpatient follow-up for low-risk mild traumatic brain injury. *World Neurosurg*. 2021;151:e565-e570.
33. Wang X, Shen T, Yang S, et al. A deep learning algorithm for automatic detection and classification of acute intracranial hemorrhages in head CT scans. *NeuroImage Clin*. 2021;32:102785.
34. Alfaer NM, Aljohani HM, Abdel-Khalek S, Alghamdi AS, Mansour RF. Fusion-based deep learning with nature-inspired algorithm for intracerebral Haemorrhage diagnosis. *J Healthcare Eng*. 2022;2022. doi:10.1155/2022/4409336
35. Rahman AI, Bhuiyan S, Reza ZH, Zaheen J, Khan TA. *Detection of Intracranial Hemorrhage on CT Scan Images Using Convolutional Neural Network* Doctoral dissertation. Brac University; 2021.

How to cite this article: Monica Jenefer BM, Senathipathi K, Aarthi, Annapandi. Detection and categorization of acute intracranial hemorrhage subtypes using a multilayer DenseNet-ResNet architecture with improved random forest classifier. *Concurrency Computat Pract Exper*. 2022;34(22):e7167. doi: 10.1002/cpe.7167